The Astrophysical Journal, 795:164 (9pp), 2014 November 10 doi:10.1088/0004-637X/795/2/164

C IV AND C III] REVERBERATION MAPPING OF THE LUMINOUS QUASAR PG 1247+267

D. Trevese[1], M. Perna[2], F. Vagnetti[3], F. G. Saturni[1,4], and M. Dadina[5]
[1] Dipartimento di Fisica, Università di Roma La Sapienza, Piazzale Aldo Moro, 5, I-00185 Roma, Italy
[2] Dipartimento di Fisica e Astronomia, Università di Bologna, Viale Berti Pichat 6/2, I-40127 Bologna, Italy
[3] Dipartimento di Fisica, Università di Roma Tor Vergata, Via della Ricerca Scientifica 1, I-00133 Roma, Italy
[4] European Southern Observatory, Karl-Schwarzschild-Strasse 2, D-85748 Garching bei München, Germany
[5] INAF-IASF Bologna, Via Gobetti 101, I-40129 Bologna, Italy
Received 2014 July 2; accepted 2014 September 16; published 2014 October 28

ABSTRACT

So far the masses of about 50 active galactic nuclei (AGNs) have been measured through the reverberation mapping technique (RM). Most measurements have been performed for objects of moderate luminosity and redshift, based on Hβ, which is also used to calibrate the scaling relation that allows single-epoch (SE) mass determination based on AGN luminosity and the width of different emission lines. Due to the complex structure and gas dynamics of the relevant emission region, the SE masses obtained from the C IV(1549 Å) line show a large spread around the mean values. Direct RM measures of C IV exist for only six AGNs of low luminosity and redshift, and only one luminous quasar. Since 2003, we have collected photometric and spectroscopic observations of PG1247+267, the most luminous quasar ever analyzed for RM. We provide light curves for the continuum and for C IV(1549 Å) and C III](1909 Å), and measures of the reverberation time lags based on the SPEAR method. The sizes of the line emission regions assume a ratio of $R_{\rm C\,III]}/R_{\rm C\,IV} \sim 2$, similar to the case of Seyfert galaxies, indicating for the first time a similar ionization stratification in a luminous quasar and low-luminosity nuclei. Due to the relatively small size of the broad line region and the relatively narrow line widths, we estimate a small mass and an anomalously high Eddington ratio. We discuss the possibility that either the shape of the emission region or an amplification of the luminosity caused by gravitational lensing may be partly responsible for the result.

Key words: galaxies: active – quasars: emission lines – quasars: general – quasars: individual (PG 1247+267) – quasars: supermassive black holes

1. INTRODUCTION

Reverberation mapping (RM) has played a crucial role in the study of the structure of active galactic nuclei (AGNs). Spectroscopic monitoring in the UV/optical band allows us to measure emission line flux changes that represent the "echo" of far-UV ionizing continuum variations, which in turn are closely related to the observed near-UV continuum variations. The delay τ_l of the echo, i.e., of line variation with respect to continuum changes, is measured through continuum-line cross-correlation and provides the luminosity-weighted average distance, $R = c \cdot \tau_l$, of the line-emitting region from the (point-like) continuum source, where c is the speed of light (Blandford & McKee 1982; Peterson 1993). Until 1999, 17 AGNs with $\lambda L_\lambda(5100\,\text{Å}) \lesssim 1.5 \times 10^{44}\,\text{erg s}^{-1}$ had been studied (see Wandel et al. 1999, and references therein), resulting in measurements of the sizes of their broad line regions (BLR) and demonstrating a stratification of ionization, with the higher ionization lines responding more rapidly to continuum changes. Combining the size, R, with a measure of the typical velocity, ΔV, of the emitting BLR clouds, assumed to be in Keplerian orbits, it is possible to derive a virial estimate of the black hole mass $M_{\rm BH} = f c \tau_l \Delta V^2/G$ of the central black hole, where G is the gravitational constant and f is a scaling factor depending on the geometry of the BLR and the specific definition adopted for ΔV (see Section 4). The extension of these results with the addition of a sample of 17 quasars (QSO) with luminosities of λL_λ(5100 Å) up to $\sim 6.5 \times 10^{45}\,\text{erg s}^{-1}$ allowed Kaspi et al. (2000) to establish a $R \propto L^\gamma$-type size–luminosity scaling relation in a luminosity range covering more than four decades (Kaspi et al. 2005; Bentz et al. 2006, 2009). This relation can be used to estimate the BH mass based on ΔV and L measured from single epoch (SE) spectra (Vestergaard 2002; McLure & Jarvis 2002), raising the possibility of estimating the BH mass of thousands of QSOs/AGNs, analyzing their luminosity function at different redshifts, and following the BH-galaxy co-evolution in cosmic time (Shen & Kelly 2012). The widths of different lines, Hβ, C IV, Mg II, are used depending on the redshift and wavelength range of optical/IR ground-based observations. However, the scaling relations for C IV and Mg II (McLure & Jarvis 2002; Vestergaard & Peterson 2006; McGill et al. 2008) are not obtained from the few direct RM measures of these lines, but are instead calibrated on the mass scale based on Hβ time lags, which represent the majority of RM measures to date. The latter are currently limited to objects with $\lambda L_\lambda(5100\,\text{Å}) \lesssim 10^{46}\,\text{erg s}^{-1}$ and $z < 0.3$ (Bentz et al. 2013, and references therein). According to Netzer (2003), the largest black hole masses deduced from these extrapolations, occurring in objects with the highest luminosities, would exceed $10^{10} M_\odot$ and, if converted to host galaxy mass and luminosity through the statistical relation between the black hole mass, galaxy bulge mass, and stellar velocity dispersion, would imply galactic bulge masses of $M_{\rm bulge} \gtrsim 10^{13} M_\odot$ and stellar velocity dispersions exceeding $700\,\text{km s}^{-1}$ which have never been observed, suggesting that either the $M_{\rm BH}$–$M_{\rm bulge}$ correlations observed in the local universe are different at higher redshift, or that the observed size–luminosity relationship in low-luminosity AGNs does not extend to very high luminosities. Vestergaard (2004) pointed out that the space density of such luminous quasars is so low that their local absence does not mean that they do not exist. In any case, exploring the validity or failure of the size–luminosity scaling relation is of crucial importance, not only to understand the physical conditions in the most luminous QSOs, but also because most of the AGN mass estimates are based on this

unconfirmed extrapolation, which could lead to uncertain or biased conclusions concerning the evolution of the AGN mass function in cosmic time. To measure the BRL size and BH mass of luminous QSOs, in 2003 we started a monitoring campaign of four high-luminosity ($L \gtrsim 5 \times 10^{46}$ erg s^{-1}) and intermediate-redshift ($2 < z < 4$) objects with the Copernico 1.82 m telescope in Asiago (Italy) and the Cassini 1.52 m telescope in Loiano (Italy). Trevese et al. (2007) published some results for the QSOs PG 1634+706, with $z = 1.337$, and PG 1247+267, with $z = 2.048$, demonstrating the detectability of the emission line variations. A study of the broad absorption line variability of the luminous quasar APM 08279+5255 (Trevese et al. 2013; Saturni et al. 2014) and preliminary results on RM for PG 1247+267 (Perna et al. 2014) were also presented.

At $z \gtrsim 2$, Hβ is no longer observable in the optical band and reverberation can be observed for the C III] (λ1909 Å) and C IV(λ1549 Å) lines. Reverberation measurements of the C IV line are available only for a handful of low-luminosity ($\lambda L_\lambda(1350\,\text{Å}) \lesssim 10^{44}$ erg s^{-1}) and low-redshift ($z < 0.06$) AGNs observed in the ultraviolet from space. In addition, Kaspi et al. (2007) presented the first results of an RM campaign begun in 1999 with the HET 11 m telescope (Ramsey et al. 1998) providing a first tentative mass estimate for S5 0836+071, a luminous ($\lambda L_\lambda(1350\,\text{Å}) = 1.12 \pm 0.16 \times 10^{47}$ erg s^{-1}) QSO at $z = 2.172$, based on C IV RM. More recently, several studies discussed the unreliability of C IV-based mass estimates, due to gas outflows strongly affecting the profile of this line (Netzer et al. 2007; Sulentic et al. 2007; Marziani & Sulentic 2012; Denney 2012). The fact that there is no consensus about the scatter and possible biases between C IV-based and Hβ-based BH masses (Greene et al. 2010; Assef et al. 2011; Runnoe et al. 2013) further increases the importance of RM measure of the size of the emitting region in order to constrain wind models and eventually lead to a consistent picture that includes the BH mass, gas outflow, and possibly its feedback on the host galaxy.

In this work, we present the C IV, C III], and continuum light curves obtained for PG 1247+267, and we estimate the relevant time lags based on a method proposed by Zu et al. (2011). We also analyze the shape of the C IV and C III] lines and discuss the determination of the virial mass of the central BH, the corresponding value of the Eddington ratio, and possible explanations of the anomalously high values found. The paper is organized as follows. In Section 2, we describe the observation and data reduction. In Section 3, we discuss the estimate of the time lags. In Section 4, we discuss the mass estimates based on C IV, C III] RM. In Section 5, we draw our conclusions.

Throughout this paper, we adopt the cosmology $H_o = 70\,\text{km s}^{-1}\,\text{Mpc}^{-1}$, $\Omega_m = 0.3$, and $\Omega_\Lambda = 0.7$.

2. OBSERVATIONS AND DATA REDUCTION

The majority of observations were carried out using the Faint Object Spectrograph and Camera AFOSC at the Copernico 1.82 m telescope in Asiago (Italy). We measured relative spectrophotometric variations by including a reference star in a wide (8.″44) slit to avoid differential flux losses caused by atmospheric refraction. The reference star is the object at $\alpha = 125011.44$, $\delta = +263332.1$ (J2000), with V = 13.824 (Pickles & Depagne 2010). At each epoch, the observations consist of two consecutive exposures of ~1800 s. The typical resolution is ~15 Å in the spectral range 3500–8500 Å. Details are described in Trevese et al. (2007). The QSO and reference star uncalibrated spectra, $Q(\lambda)$ and $S(\lambda)$, respectively, are extracted by the standard IRAF[6] procedures, and the ratio $\mu^{(k)} = Q^{(k)}(\lambda)/S^{(k)}(\lambda)$ is computed for each exposure $k = 1, 2$. This quantity is independent of extinction variations and allows us to reject inconsistent exposure pairs whenever $|\mu^{(2)}/\mu^{(1)} - 1|$ averaged over 500 Å exceeds 0.04. This procedure also allows us to compute the relative flux differences between the two exposures, which are used to estimate the statistical errors on continuum and emission line fluxes. At the ith epoch t_i, pairs of spectra for both the QSO and the reference star were co-added to compute the ratio $\mu_i(\lambda) = Q_i(\lambda)/S_i(\lambda) = (Q^{(1)} + Q^{(2)})/(S^{(1)} + S^{(2)})$. Data separated by less than one day are combined into a single epoch data point.

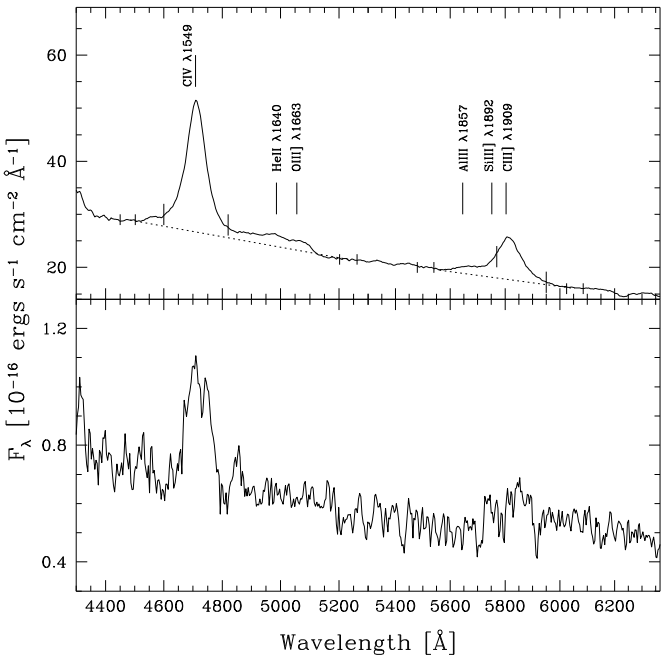

Figure 1. Upper panel: average spectrum of PG 1247+267 from our observations. Spectral ranges selected for the determination of the local continua (short ticks) and for the line flux (long ticks) are marked on the spectrum. Dotted lines represent the interpolated local continuum. Lower panel: rms spectrum as defined in Peterson et al. (1998).

The flux-calibrated spectrum of the star $F^S(\lambda)$ was obtained at a single reference epoch and the calibrated quasar spectra were obtained for each epoch as $F_i^Q(\lambda) = \mu_i(\lambda)F^S(\lambda)$. We stress that the spectra are independent of extinction changes and detector response, and thus spectral variations are also independent of telescope, detector, and calibration. This allows us to include four spectra taken at the 1.5 m Cassini telescope of the Loiano Observatory with the BFOSC camera. At each epoch, two exposures of 2700 s were taken with about the same resolution of AFOSC spectra.

Although the following reverberation analysis is independent of the absolute calibration, we have now revised the calibration of the spectra for possible future uses. This has been done by multiplying the calibrated spectrum of the reference star by a constant factor which makes its V magnitude, as computed from the spectrum adopting the Bessell (1990) filter profile, equal to V = 13.824 as given by Pickles & Depagne (2010).

Figure 1 shows the flux-calibrated average spectrum and the rms spectrum of PG 1247+267. A spectral decomposition of

[6] IRAF is distributed by the National Optical Astronomy Observatory, which is operated by the Association of Universities for Research in Astronomy, Inc., under cooperative agreement with the National Science Foundation.

the Al III +Si III] + C III] blend indicates an Si III]/C III] flux ratio of $\lesssim$0.3. This is consistent with the corresponding ratio reported in Table 2 of Bachev et al. (2004), since PG 1247+267 belongs to class B of Sulentic et al. (2002) based on the FWHM of the broad component of its Hβ line (7460 $\pm$ 220 km s^{-1}) as measured by McIntosh et al. (1999). The integration limits adopted further reduce by a factor of $\sim$2 the contribution to the computed C III] flux of Si III], which has therefore been neglected. Similarly, the adopted continuum and integration limits should avoid the contamination of C IV flux from the He II(1640 Å) and O III](1663 Å) emission. The lower panel of Figure 1 shows the rms spectrum. As expected, it appears more noisy than the average spectrum (see Denney 2012). Nonetheless, in the case of the stronger line C IV, the average and rms profiles appear similar (see Section 4).

Line fluxes are computed as $f_l = \int_{\lambda_1}^{\lambda_2}[F^{(Q)}(\lambda) - c^{\rm int}(\lambda)]d\lambda$, where $c^{\rm int}(\lambda)$ is the linear interpolation through the continua at shorter and longer wavelengths of each line, $\lambda_{\rm short}$ and $\lambda_{\rm long}$ indicated in Figure 1, and the extremes of integration λ_1 and λ_2 are chosen to optimize the f_l signal-to-noise ratio and do not necessarily coincide with $\lambda_{\rm short}$ and $\lambda_{\rm long}$ (see Trevese et al. 2007).

The uncertainties on line fluxes are estimated by computing the flux difference $\delta = |f^{(2)} - f^{(1)}|$ between two exposures taken at the same epoch. Since the exposure time is roughly constant at all epochs and fluxes are computed as the average between two exposures, we adopt as our uncertainty on the flux $\sigma_f = \langle\delta^2\rangle^{1/2}/2$, where the angular brackets indicate the average over the entire set of measurements. The fractional values of σ_f for continuum, C III], and C IV fluxes are 0.008, 0.021, and 0.015, respectively. Direct photometry of the field was also obtained at most epochs to obtain an independent measure of the quasar luminosity changes relative to the reference star, and to check the stability of the reference star against other objects in the field. Typically, at each epoch, R-band photometry was obtained with exposures of 400 s at the Asiago Observatory. Photometry is also available in the *R* and/or *V* bands, from the Loiano Observatory.

From the average spectrum, we can estimate that the contribution of the C III] line to the R and V magnitudes is about 0.04 mag and 0.03 mag, respectively, while the contribution of C IV is negligible in both bands. Thus, we can use photometric data to measure continuum variations without significantly altering the continuum-line cross-correlation function. In doing this, we convert V magnitudes to R' magnitudes assuming R'(V) $\equiv$ V-$\langle$V-R$\rangle$, where the angular brackets indicate the average over those epochs when both R and V are measured. This conversion assumes that the V-R quasar color is constant. We have checked that rms color changes are of the order of 0.007 mag. Such color changes could slightly affect the amplitude of the continuum-line cross-correlation only in the case of C III], but cannot significantly affect the estimate of the time delay. A measure of the continuum changes can also be obtained from the spectra. This has been achieved by fitting with a single straight line, $\log F^{\rm cont}(\lambda) = -a\log\lambda + b$, the four data points that define the local continua (shown in Figure 1). From these fits, we have identified a conventional spectral continuum at the peak wavelength of the Bessell (1990) *V* band, $F_C \equiv F_\lambda^{\rm cont}(5300\,\text{Å})$. For the subsequent analysis (see Section 3), continuum flux changes were referred to the epoch t_{ref} (MJD = 53047.5) and expressed as magnitude changes $\delta m_C(t_i) = 2.5\log[F_C(t_i)/F_C(t_{ref})]$. A similar process was used for line fluxes. Continuum changes obtained from broadband photometry have been reduced to the same scale defining $\delta R(t_i) = \Delta R(t_i) + \langle\delta m_C - \Delta R\rangle$, where the average is taken over all the epochs when both photometric and spectroscopic data are available.

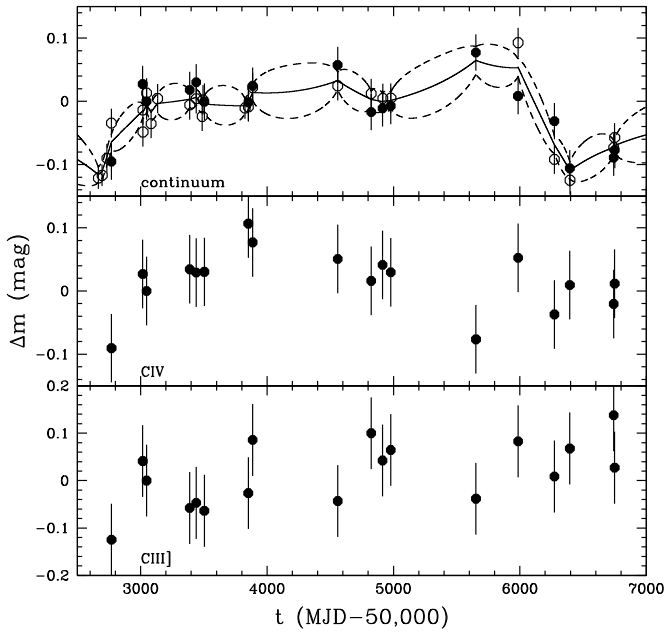

Figure 2. Magnitude changes as a function of time. Upper panel: continuum changes from spectrophotometry δm_C (filled circles) and from broadband photometry δR (open circles). Data interpolation (continuous line) and the relevant 1σ uncertainty (dashed lines) according to the method of Zu et al. (2011). Middle panel: C IV(1549 Å) line. Bottom panel: C III](1909 Å) line.

Table 1 reports the results. Column 1 presents the date, Column 2 presents the Modified Julian Date (MJD), Column 3 indicates the telescope, Columns 4 and 5 present the V- and *R*-band magnitude differences with respect to the reference star, Column 6 presents the continuum changes δR obtained from broadband photometry, Column 7 presents the continuum specific flux F_C at $\lambda = 5300$ Å, and Columns 8 and 9 present the C III and C IV] line fluxes, respectively.

Figure 2 reports the light curves in magnitude for the continuum and emission lines.

3. MEASURING THE REVERBERATION TIME LAGS

The time lag τ_l of the emission line variation with respect to continuum changes is measured by the centroid of the continuum-emission line cross-correlation function, which can be computed using the discrete correlation function (DCF; Edelson & Krolik 1988) or by interpolating the light curves (Gaskell & Peterson 1987; White & Peterson 1994). Both methods provide consistent results for well-sampled light curves. In the case of poor sampling, both methods present technical problems (see the review by Peterson 1993). In particular, the DCF becomes less sensitive to real correlations. Moreover, the estimate of a confidence interval on the measured time lag, which can be obtained by the z-transform method developed by Alexander (1997), requires us to eliminate from each DCF bin all of the points corresponding to pairs of epochs having a measure in common. This causes us to lose part of the information contained in the data, and so the method may be not applicable if the total number of observations is too small.

We adopt a methodology called the Stochastic Process Estimation for AGN Reverberation (SPEAR) developed by Zu et al. (2011). The statistical basis of the method was introduced by Press et al. (1992) and Rybicki & Press (1992). A subsequent

Table 1
Variability Measurements for PG 1247+267

Date	MJD	Telescope[a]	ΔV	ΔR	δR	$F_\lambda^{\rm cont}$(5300 Å)	$f_{\rm C\,III]}$	$f_{\rm C\,IV}$
			magnitudes			(10^{-15} erg cm^{-2} s^{-1} Å^{-1})	(10^{-14} erg cm^{-2}s^{-1})	
03-01-25	52665.3	L	1.660 ± 0.003	···	-0.122 ± 0.017	···	···	···
03-02-23	52694.5	L	1.665 ± 0.003	···	-0.117 ± 0.017	···	···	···
03-04-01	52733.4	L	1.696 ± 0.003	1.80 ± 0.01	-0.090 ± 0.023	···	···	···
03-05-09	52769.3	A	···	1.83 ± 0.01	-0.034 ± 0.023	2.34 ± 0.02	8.2 ± 0.2	25.6 ± 0.4
04-01-13	53017.6	A	···	1.85 ± 0.01	-0.014 ± 0.023	2.09 ± 0.02	7.0 ± 0.1	23.0 ± 0.3
04-01-14	53018.6	A	···	1.82 ± 0.01	-0.048 ± 0.023	···	···	···
04-02-12	53047.5	A	···	1.88 ± 0.01	0.013 ± 0.023	2.15 ± 0.02	7.3 ± 0.2	23.6 ± 0.4
04-03-18	53083.0	L	1.758 ± 0.003	1.83 ± 0.01	-0.035 ± 0.023	···	···	···
04-05-07	53133.9	L	1.780 ± 0.003	1.87 ± 0.01	0.004 ± 0.023	···	···	···
05-01-17	53388.6	A	···	1.86 ± 0.01	-0.006 ± 0.023	2.11 ± 0.02	7.7 ± 0.2	22.8 ± 0.3
05-03-10	53439.6	A	···	1.87 ± 0.01	0.004 ± 0.023	2.09 ± 0.02	7.6 ± 0.2	23.0 ± 0.3
05-04-26	53487.4	L	1.762 ± 0.003	1.84 ± 0.01	-0.024 ± 0.023	···	···	···
05-05-02	53493.5	L	1.775 ± 0.003	1.87 ± 0.01	0.002 ± 0.023	···	···	···
05-05-13	53503.5	A	···	···	···	2.15 ± 0.02	7.7 ± 0.2	22.9 ± 0.4
06-03-31	53826.4	L	1.771 ± 0.003	1.86 ± 0.01	-0.010 ± 0.017	···	···	···
06-04-26	53852.5	A	···	1.86 ± 0.01	-0.009 ± 0.023	2.15 ± 0.02	7.5 ± 0.2	21.4 ± 0.3
06-05-30	53886.5	A	···	1.89 ± 0.01	0.022 ± 0.023	2.10 ± 0.02	6.8 ± 0.1	22.0 ± 0.3
08-04-02	54559.4	A	···	1.89 ± 0.01	0.025 ± 0.023	2.04 ± 0.02	7.6 ± 0.2	22.5 ± 0.3
08-12-23	54823.7	A	···	1.88 ± 0.01	0.012 ± 0.023	2.18 ± 0.02	6.7 ± 0.1	23.2 ± 0.3
09-03-23	54915.7	A	···	1.87 ± 0.01	0.005 ± 0.023	2.17 ± 0.02	7.0 ± 0.1	22.7 ± 0.3
09-05-27	54979.5	A	···	1.87 ± 0.01	0.005 ± 0.023	2.16 ± 0.02	6.9 ± 0.1	23.0 ± 0.3
11-04-01	55652.5	A	···	···	···	2.00 ± 0.02	7.6 ± 0.2	25.3 ± 0.4
12-02-27	55985.5	A	···	1.96 ± 0.01	0.093 ± 0.023	2.13 ± 0.02	6.8 ± 0.1	22.5 ± 0.3
12-12-11	56272.7	L	···	1.78 ± 0.01	-0.092 ± 0.023	2.21 ± 0.02	7.2 ± 0.2	24.4 ± 0.4
13-04-13	56396.4	L	···	1.74 ± 0.01	-0.125 ± 0.023	2.37 ± 0.02	6.9 ± 0.1	23.4 ± 0.4
24-03-14	56741.6	L	···	1.80 ± 0.01	-0.073 ± 0.023	2.33 ± 0.02	6.4 ± 0.1	24.0 ± 0.4
01-04-14	56749.5	L	···	1.81 ± 0.01	-0.057 ± 0.023	2.31 ± 0.02	7.1 ± 0.1	23.3 ± 0.4

Note. [a] A: Copernicus telescope, Asiago; L: Cassini telescope, Loiano.

modification and application to the RM of NGC 5548 is discussed in Rybicki & Kleyna (1994). For a detailed description of SPEAR, we refer the reader to the paper of Zu et al. (2011). An upgraded version, called JAVELIN, which allows photometric RM, is discussed in Zu et al. (2013a). Here, we recall a few important points that motivated our choice to adopt this method to measure reverberation time lags in our case. First of all, this method makes use of interpolation, which is essential for us given the small number of data points. However, while a simple linear interpolation is based on two nearby points, here the entire data set contributes to each interpolated point through weights which are statistically determined from the correlation functions of the data. Moreover, statistical uncertainties are assigned to each interpolated value. The uncertainties tend toward the measurement errors in proximity to the data points, and become increasingly larger when the distance from the neighboring data points increases (see Figure 2). The main assumption of this method is that the emission-line flux variations $l(t)$ are scaled, smoothed, and time-shifted versions of the continuum variations $c(t)$, obtained through a transfer function $\Psi(t)$:

$$l(t) = \int dt' \Psi(t') c(t - t'). \quad (1)$$

In our analysis, for $\Psi(t)$ we assume the simple form adopted by Zu et al. (2011):

$$\Psi(t) = A/\Delta, |t - \tau_l| \leqslant \Delta; \quad \Psi(t) = 0 \text{ elsewhere}, \quad (2)$$

where A, τ_l, and Δ represent the attenuation, line-continuum lag, and the temporal width, respectively. A maximum likelihood code determines the attenuation, smoothing, and time lag parameters. The resulting emission line delay τ_l does not depend strongly on the form assumed for $\Psi(t)$ (Rybicki & Kleyna 1994). The correlation functions of the data are represented by parametric models whose parameters are also determined by likelihood maximization. This allows us to add information deduced from existing data on the statistical properties of QSO light curves. In fact, it has been shown that a damped random walk (DRW) process is a good representation of QSO variability (Kelly et al. 2009; Kozłowski et al. 2010; MacLeod et al. 2010; Zu et al. 2013b). The DRW auto-correlation function of the continuum changes $c(t)$ has the following form:

$$\langle c(t) c(t + \tau_l) \rangle = \sigma^2 \exp(-|\tau_l|/\tau_d), \quad (3)$$

where τ_l is a time lag, τ_d is the damping timescale, σ is the variability amplitude, and the angular brackets indicate the ensemble average. Another important feature of the SPEAR method is that the light curves of more lines can be included in the same fitting procedure. This provides more stringent constraints that allow for a better choice among the local likelihood maxima in the parameter space.

A single fitting procedure determines the eight parameters: σ and τ_d for the continuum, the time lags $\tau_{\rm C\,IV}$ and $\tau_{\rm C\,III]}$, the amplitudes $A_{\rm C\,IV}$ and $A_{\rm C\,III]}$, and the smoothing parameters $\Delta_{\rm C\,IV}$ and $\Delta_{\rm C\,III]}$ for the two lines, respectively. SPEAR adopts a Bayesian method to determine the confidence interval in the parameter space. Once the values of the parameters maximizing the likelihood are determined, random increments obtained from *prior* statistical distributions are applied to all of the parameters and the likelihood is re-evaluated. Following

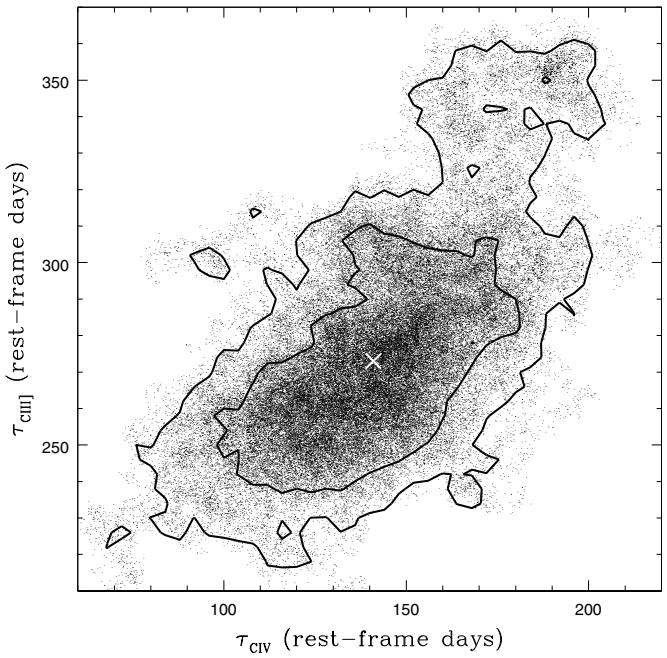

Figure 3. Distribution of points generated by 10^5 MCMC iterations in the ($\tau_{\rm C\,IV}$,$\tau_{\rm C\,III]}$) plane. Contours correspond to 68% and 95% confidence levels. The white cross indicates the median values of the marginal distributions of the two parameters.

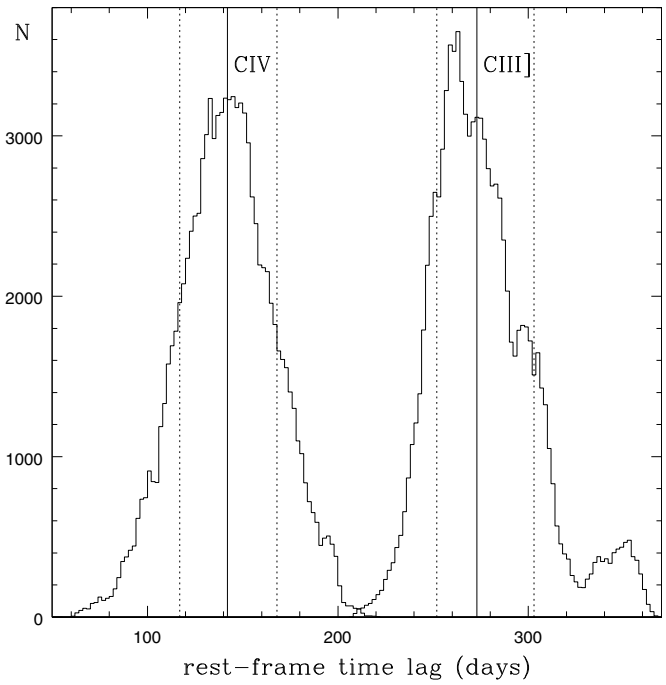

Figure 4. Posterior distributions of the rest-frame time lags $\tau_{\rm C\,IV}$ and $\tau_{\rm C\,III]}$ produced by the SPEAR method with 10^5 MCMC iterations. The continuum vertical lines indicate the median values and the dashed lines indicate the 68% confidence intervals.

a Markov Chain Monte Carlo (MCMC) method (see Press et al. 2007, and references therein), the process is iterated and a *posterior* distribution of the acceptable parameters is produced. Figure 3 shows the distribution of points in the ($\tau_{\rm C\,IV}$,$\tau_{\rm C\,III]}$) plane after 10^5 MCMC iterations, and the corresponding 68% and 95% confidence regions. Figure 4 shows the relevant posterior distributions obtained separately for $\tau_{\rm C\,IV}$ and $\tau_{\rm C\,III]}$. From these, we take their median values as a fiducial estimate of the fitting parameters, with the uncertainties defined by the 68% confidence intervals: $\tau_{\rm C\,IV} = 142 \pm ^{26}_{25}$ days and $\tau_{\rm C\,III]} = 273 \pm ^{30}_{21}$ days in the QSO rest-frame.

With respect to our preliminary results (Perna et al. 2014), the present analysis differs because (1) we simultaneously fit both the C IV and C III] light curves, (2) the continuum light curve includes the available V- and *R*-band photometry, together with the continuum variations measured from the spectra, and (3) we have included photometric and spectroscopic data of the three most recent epochs. Considering the small number of points and the uneven sampling, with two main gaps for MJD (53900, 54500) and MJD (55000, 55600), it is worth questioning whether the likelihood maxima are real or are determined by the sampling pattern. To this end, we performed a Monte Carlo simulation, generating $N = 1000$ mock, uncorrelated, continuum and emission line light curves, assuming the same set of sampling epochs, rms variability amplitudes, and measurement uncertainties. We applied the SPEAR procedure to the kth set of light curves and, once σ and τ_d were fitted, we produced a likelihood "image" $\mathcal{L}_k(\tau_l, \Delta_l)$ as a function of the lag τ_l and the smoothing parameter Δ_l, (l = CIV, CIII]). Then, we analyzed the sum $\mathcal{L} \equiv \Sigma_{k,1}^{N} \mathcal{L}_k$, which must show the local maxima corresponding to the points (τ_l, Δ_l) where maxima occur more frequently in the simulations, and thus indicating the effect of the fixed sampling pattern. The result shows that local maxima do exist but, with respect to the case of real data, (1) they are confined to much lower values of $\Delta_{\rm C\,IV}$ and $\Delta_{\rm C\,III]}$, (2) they are less pronounced, and, most important, (3) they are not located in the same position of the ($\tau_{\rm C\,IV}$-$\tau_{\rm C\,III]}$) plane where they occur in the case of real data.

We can conclude that it is very unlikely that the local maxima related to the sampling pattern produce the maxima obtained in the case of the measured light curves. Thus, we assume this result as first evidence that the values of $\tau_{\rm CIV}$ and $\tau_{\rm C\,III]}$ for PG 1247+267 are due to real echo lags.

We can compare them with the few corresponding RM results available in the literature. Measures of both the C IV and C III] time lags from RM exist for three Seyfert nuclei: NGC 5548 (Peterson & Wandel 1999), NGC 3783 (Onken & Peterson 2002), and NGC 4151 (Metzroth et al. 2006, and references therein), which are all less luminous than $\lambda L_\lambda(1350\,\text{Å}) \approx 4 \times 10^{43}\,\text{erg s}^{-1}$. On average, the ratio of the time lags of these two lines is $\tau_{\rm CIII}/\tau_{\rm CIV} \approx 2$. While there is no reason to expect that a QSO, 10^4 times more luminous, should show approximately the same ratio, it is interesting to note that in the case of PG 1247+267, we obtain $\tau_{\rm CIV}/\tau_{\rm CIII]} \sim 2$, i.e., the typical distance from the continuum source of the emission region of the semi-forbidden C III] line is about twice the distance of the C IV emission region. The situation is summarized in Figure 5 where we also report the relevant time lags for the QSO 2237+0305 as we deduced from the results of Sluse et al. (2011), who estimate the size of the C IV and C III] emission regions based on microlensing. The corresponding point looks roughly consistent with the general trend, despite the relevant sizes being of the order of 100 times larger than those of Seyfert galaxies. A straight line fit to the data points in Figure 5, $\log \tau_{\rm C\,III]} = a \log \tau_{\rm C\,IV} + b$, gives $a = 0.83 \pm 0.21$ and $b = 0.43 \pm 0.19$. A fit with fixed unitary slope gives $\tau_{\rm C\,III]}/\tau_{\rm C\,IV} = 1.8 \pm 0.5$. The very existence of this relation can be taken as a second suggestion that we are probably measuring real reverberation time lags. This result would mean that the ionization stratification in Seyfert nuclei and luminous quasars is similar.

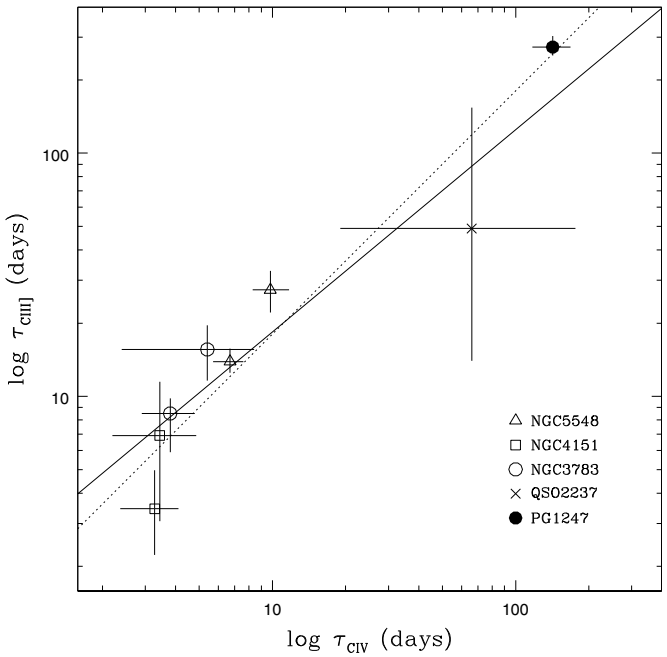

Figure 5. Reverberation time lags $\tau_{\rm CIII}$ vs. $\tau_{\rm CIV}$ for NGC 5548, NGC 3783, NGC 4151, and PG 1247+267 (our estimate). The emission region sizes (Sluse et al. 2011), converted to time lags, are also reported for the quasar QSO 2237+0305. Straight lines represent linear fits with errors on both variables: the continuous line with two free parameters and the dotted line with fixed unitary slope.

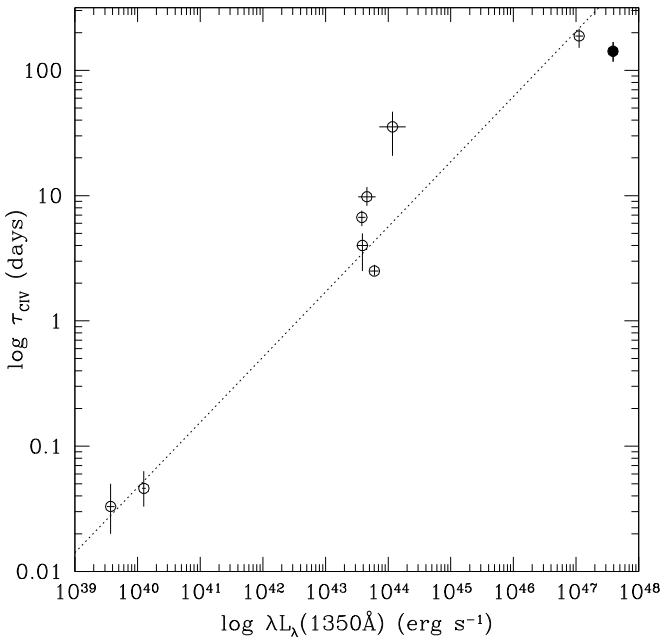

Figure 6. Size–luminosity relation obtained from the C IV emission line and UV continuum. Open circles: data from Peterson et al. (2005, 2006) plus the values for S5 0836+71 from Kaspi et al. (2007). Filled circle: our result for PG 1247+267. The dotted line represents the linear fit obtained by Kaspi et al. (2007) using the FITEXY method (Press et al. 1992).

Figure 6 shows the relation between the emission radii $R_{\rm C\,IV} = c\tau_{\rm C\,IV}$ and the luminosity $\lambda L_\lambda(1350$ Å) for all the objects studied so far. For their second brightest object S5 0836+071, Kaspi et al. (2007) give $\lambda L_\lambda(1350\,\text{Å}) = 1.12 \pm 0.16 \times 10^{47}$ erg s^{-1} and a tentative value of the C IV emission line delay of $\tau_{\rm C\,IV} = 188\pm^{27}_{37}$ days in the quasar rest frame. They also discuss the slope of the $\tau_{\rm C\,IV} - \lambda L_\lambda$ relation obtained using different fitting procedures. The fit they obtain with the FITEXY algorithm (Press et al. 1992), shown in Figure 6, corresponds to a slope of $\gamma = 0.52 \pm 0.04$.

PG 1247+267 is the brightest QSO ever analyzed for reverberation and has $\lambda L_\lambda(1350\,\text{Å}) = 3.92 \pm 0.02 \times 10^{47}$ erg s^{-1}, deduced from Shen et al. (2011), and thus it is 3.5 times more luminous than S5 0836+071. Compared with the extrapolation of the lag–luminosity relation in Figure 6, PG 1247+267 should show a reverberation lag of about 400 days, i.e., ∼3 times larger than observed. If confirmed, then this would imply a decrease of about 10% of the slope γ of the $\tau_{\rm C\,IV} - \lambda L_\lambda$ relation, whose significance is marginal, however, due to the relatively large dispersion of the still small number of points in the lag–luminosity diagram for C IV. In the case of S5 0836+71, Kaspi et al. (2007) obtain $\tau_{\rm C\,III]}$ consistent with zero. A possible explanation may be that they do not use an interpolation of the light curves, which becomes necessary when the total number of points is small.

4. ESTIMATING THE VIRIAL MASS

From the emission radii $R_{\rm C\,IV} = c\tau_{\rm C\,IV}$ and $R_{\rm C\,III]} = c\tau_{\rm C\,III]}$, we can try and measure the BH mass through the virial relation. Unfortunately, the use of the C IV emission line for mass estimation appears to be problematic (Netzer et al. 2007) since the profile of this line reveals the contribution of different components whose relative weights vary so much from object to object that the shape of this line turns out to be a good indicator of different AGN types (Sulentic et al. 2007). In principle, the velocity ΔV appearing in the virial relation $M_{\rm BH} = f R\Delta V^2/G$ could be identified using the FWHM of the emission line or with the rms velocity dispersion along the line-of-sight σ_l (Peterson et al. 2004).

Under the assumption of an isotropic velocity field, the kinetic energy is $K = 3/2 M\sigma_l^2$ but the numerical factor may differ from 3/2 depending on anisotropies, possibly related to the shape of the broad line clouds system. Consequently, the numerical factor can be different for different emission lines, even in the same AGN. In the case of a Gaussian line profile, FWHM$/\sigma_l = 2.35$ but may be different for different profiles. All of the numerical factors are absorbed in the factor f of the virial relation and contribute to the uncertainty of the mass determination, both in the case of RM and SE measurements. In RM experiments where several spectra taken at different times are available, it is possible to compute the rms spectrum (Peterson et al. 1998).

The non-variable parts of the spectrum, or those which vary on timescales much longer than the experiment, do not contribute to the rms spectrum. The rms spectrum of PG 1247+267 is shown in the lower panel of Figure 1. The uncertainty on σ_l can be computed by applying a bootstrap procedure described in Peterson et al. (2004). The reason to use the rms instead of the average spectra is to avoid (1) the underestimates of ΔV caused by the narrow emission line component and (2) the effect of non-virial outflows, which are expected to vary on timescales longer than reverberation time lags (see Denney 2012).

Our results are summarized in Table 2 where the reverberation time lags for both C IV and C III] are reported, along with the relevant FWHM and σ_l computed from the mean and rms spectra. The virial products $\tau_{\rm C\,IV}\Delta V^2_{\rm C\,IV}$ and $\tau_{\rm C\,III]}\Delta V^2_{\rm C\,III]}$ appear to be consistent with the same black hole mass. We assume this fact as a third piece of evidence that we are measuring real reverberation lags.

Table 2
Reverberation Results for PG 1247+267

Emission line	τ_l[a]	FWHM$_{mean}$	$\sigma_{l,mean}$	FWHM$_{rms}$	$\sigma_{l,rms}$
	days	km s^{-1}			
C IV λ1549	142^{+26}_{-25}	4939 ± 117	2673 ± 20	4568 ± 1338	2104 ± 540
C III] λ1909	273^{+30}_{-21}	5224 ± 63	2365 ± 15	4752 ± 1156	1899 ± 713

Note. [a] In the rest frame

Table 3
Mass Estimates for PG 1247+267

Emission line	M_{BH}^{mode}	M_{BH}^{cent}
	$10^8 M_\odot$	
C IV λ1549	$6.7^{+5.0}_{-1.1}$	$\mathbf{8.3}^{+3.4}_{-2.7}$
C III] λ1909	$10.5^{+17.2}_{-9.1}$	$9.9^{+17.8}_{-8.5}$

The numerical factor f in the virial relation can be determined empirically by calibrating the RM masses through the M_{BH}–σ_* relation (Ferrarese & Merritt 2000), as done for Hβ RM by Onken et al. (2004), who finds $f = 5.5$. From the calibrated Hβ RM masses, Vestergaard & Peterson (2006) computed statistical scaling relations permitting SE mass determinations based on the luminosity L_λ(5100 Å) and Hβ line width. Scaling relations for SE mass determination based on the L_λ(1350 Å) and C IV line widths, normalized to the Hβ masses, are also provided. However, as mentioned above, the C IV line shape varies from object to object, and this causes a large spread in the measured masses around the scaling relation. A more accurate relation can be obtained by analyzing the line shape parameter $S = FWHM/\sigma_l$ as computed both from the average spectrum and from the rms spectrum $\sigma(\lambda)$: S_{mean} and S_{rms}, respectively. Denney (2012) pointed out that while the ratio S_{mean}/S_{rms} is of the order of one for the Hβ line, it is different for different values of S_{mean} in the case of C IV (see her Figure 2). This is interpreted in terms of an outflowing, non-reverberating component that is not contributing to the rms spectrum. A correction, dependent on S_{mean}, is proposed to reduce the masses derived from C IV to those derived from Hβ (Equation (1) in Denney (2012)): $\log M_{CIV}^{corr} = \log M_{CIV}^{orig} + 0.219–1.63 \log(FWHM_{CIV}/\sigma_{CIV})$.

In the case of PG 1247+267, $S_{mean} = 1.85$ and the value of $S_{rms}/S_{mean} = 2.2/1.85 = 1.18$ is close to one, which means that the use of the rms spectrum does not much change the value of S; namely, the effect of a non-reverberating component, though present, is small. This quantifies the similarity of the C IV emission line in the average and rms spectra, already noted in Figure 1. It is interesting to note that S5 0836+071 has $S_{mean} = 1.94$ (instead of 1.85), indicating that the shapes of the C IV lines of the two objects are similar. This suggests that the relevant virial factors f are also similar, so that the ratio of the masses is approximately the ratio of the virial products $\tau_l \Delta V^2$, whatever the definition of ΔV.

For the luminous quasar S5 0836+071 with $\lambda L_\lambda(1350\,Å) = 1.12 \pm 0.16 \times 10^{47}$ erg s^{-1}, Kaspi et al. (2007) obtained $\tau_{CIV} = 188 \pm 27$ days in the rest-frame. They define ΔV as the FWHM$_{mean}$ and, using $f = 3/4$ in Equation (2) of Kaspi et al. (2000), they obtain a mass of $M_{BH} \sim 2.6 \times 10^9 M_\odot$, which corresponds to a virial product of $c\tau_{CIV}\Delta V_{CIV}^2 \sim 3.5 \times 10^9 M_\odot$. Adopting the same definition for ΔV, for PG 1247+267 we obtain $M_{BH} \sim 6.7 \times 10^8 M_\odot$, i.e., about five times smaller despite its higher luminosity.

Using the value of σ_l obtained from the rms spectra as the definition of ΔV, Onken et al. (2004) obtained an average virial factor of $f = 5.5$. More recent estimates (see Pancoast et al. 2013, and references therein) provide different values, but we conventionally adopt the more commonly used $f = 5.5$ for the subsequent comparison with the literature. Based on this calibration and using σ_l obtained from the rms spectrum (see Table 2), we obtain $M_{BH} \sim 6.7 \times 10^8 M_\odot$.

We stress that since the distribution of ΔV^2 and τ_l is asymmetric, some care is needed when deriving the fiducial mass values and the relevant confidence intervals. For this purpose, we computed a probability distribution of the virial product, as a function of ΔV^2 and τ_l, by multiplying the posterior distribution of τ_l (see Figure 4) and the statistical distribution of ΔV^2 obtained using the bootstrap method. From this, we derived a posterior distribution of the black hole mass. In addition to the modal mass value M_{BH}^{mode}, in Table 3 we report the value computed as the centroid of the posterior distribution, together with the asymmetric errors at the 68% confidence level. Hereafter, we will use $M_{BH}^{cent} = 8.3^{+3.4}_{-2.7} \times 10^8 M_\odot$ as our best estimate of the virial mass (in bold face in Table 3). The corresponding mass values obtained from C III] are also reported in Table 3.

We can compare our result with the summary of BH masses, known from RM, versus λL_λ(1350 Å), shown in Figure 5 of Chelouche et al. (2012). Based on this comparison, it appears that the new point that we are adding at the highest luminosity corresponds to a mass which is roughly a factor of 20 smaller with respect to the extrapolation of the general trend, which would predict a mass of the order of $2 \times 10^{10} M_\odot$. The scatter of points around the M_{BH}–λL_λ(1350 Å) relation is partly intrinsic, due to the fact that different AGNs may be emitting at different Eddington ratios, and partly caused by the uncertainty on the f factor appropriate for individual objects. Thus, a deviation from the average scaling relation of a factor of ∼20 is not surprising. However, it does deserve further discussion.

5. DISCUSSION AND SUMMARY

The number of spectral observations is still small and deriving any conclusion requires caution. However, three independent circumstances suggest that we are probably measuring real reverberation time lags: (1) although it is reasonable to expect that the likelihood maxima might be determined by the uneven temporal sampling, Monte Carlo simulations with mock random light curves and the same sampling pattern do not produce likelihood maxima in the same region of the parameters space; (2) the measured C IV and C III] reverberation time lag appears to be consistent with the τ_{CIV}–$\tau_{CIII]}$ relation derived from the data available in the literature; and (3) the virial products for the C IV and C III] lines appear to be consistent with the same black hole mass.

Thus, assuming that the measured $\tau_{CIII]}$ and τ_{CIV} are real, we can derive some tentative conclusions.

The fact that the approximate relation $\tau_{CIII]} \sim 2\tau_{CIV}$ (see Figure 5) extends for objects with a luminosity of λL_λ(1350 Å) from $\approx 4 \times 10^{39}$ to $\approx 4 \times 10^{47}$ erg s^{-1}, if confirmed, would be the first direct evidence that the ionization stratification in luminous QSOs is similar to that found in Seyfert galaxies.

The relatively small τ_{CIV}, about 0.3 of the value expected from the extrapolation of the $\tau_l - L$ relation, tends to produce a small virial mass. The problem is made more severe by the

small value of the line widths, roughly two-thirds of that of S5 0836+071, which is 3.5 times less luminous. This appears clearly when we compute the Eddington ratio $L_{\rm bol}/L_{\rm Edd}$, which contains a further uncertainty deriving from the estimate of the bolometric correction. Kaspi et al. (2007) adopt the bolometric correction of Marconi et al. (2004) (Equation (21)) which refers to the luminosity $\nu_B L_{\nu B}$. For PG 1247+267, we obtain $\nu_B L_{\nu B} = 2.0 \times 10^{47}\,{\rm erg\,s^{-1}}$, interpolating between the values of $\lambda L_\lambda(2500\,\text{Å})$ and $\lambda L_\lambda(5100\,\text{Å})$ provided by Krawczyk et al. (2013). The resulting correction is $L_{\rm bol}/\nu_B L_{\nu_B} = 5.28$, leading to $L_{\rm bol} = 1.06 \times 10^{48}\,{\rm erg\,s^{-1}}$ and $L_{\rm bol}/L_{\rm Edd} = 9.8$ (after a small correction for the different cosmology we adopt). A similar result, $L_{\rm bol}/L_{\rm Edd} \sim 10.4$, is found after adopting the bolometric correction of $L(1\mu - 2\,{\rm keV})/\nu L_\nu(2500\,\text{Å}) = 3.5$ with $\log \nu L_\nu(2500\,\text{Å}) = 47.50$ from Krawczyk et al. (2013).

We stress that this large Eddington ratio is due only in part to the small size of the BLR. In fact, even the SE mass estimate, which is independent of reverberation lag, for PG 1247+267 produces an Eddington ratio in the range 1.2–3, depending on the use of the line shape correction (Denney 2012) and the different choices of bolometric correction.

As discussed in the previous section, one possible origin of a line width that is too small may be the presence of a narrow emission line component or the contribution of a possibly non-variable and non-virial wind component. This suggests using the rms spectrum. Besides this, the orbits of BLR clouds are unlikely to be randomly oriented, as suggested by various evidence reviewed by Gaskell (2009), and sources viewed at a low inclination angle (nearly face-on) show a small FWHM, leading to a systematic underestimation of the black hole mass by a factor of up to ∼10 (Marziani & Sulentic 2012).

For five Seyfert nuclei, Pancoast et al. (2013) computed line profile models that depend on the opening angle of the cloud distribution for different values of the inclination angle with respect to the axis of the accretion disk. The relevant virial factor f, to be applied when using σ_l from the rms spectra, can be as high as 50 for an inclination angle of 8 degrees. Thus, a plausibly high value of the virial factor f could easily bring the Eddington ratio toward more common values, without, however, explaining the relatively small reverberation time lag.

The effects of orientation on the characteristics of the C IV line have been investigated by Runnoe et al. (2014). By comparison with their Figure 3, the small amplitude relative to Si IV and the narrow line width found in the spectrum of PG 1247+267 in fact suggest a small inclination angle, supporting a high-f value. However, more quantitative evidence would require, a dynamical modeling of the type presented by Pancoast et al. (2013), and a comparison with velocity-resolved RM, which is not feasible with our present data.

A different, and apparently trivial, explanation for the high Eddington ratio may be an overestimate of the luminosity caused by gravitational lensing. At the same time, allowing for magnification would justify the apparently small BLR size. Moreover, we suggest taking into account two other concurrent clues. The first clue concerns the negative correlation between $\alpha_{ox} = 0.384 \log L_\nu(2{\rm keV})/L_\nu(2500\,\text{Å})$ and $L_\nu(2500\,\text{Å})$ found in statistical samples of QSOs/AGNs. With respect to this relation, PG 1247+267, with $\alpha_{ox} = -1.69$ and $L_\nu(2500\,\text{Å}) = 2.5 \times 10^{47}\,{\rm erg\,s^{-1}}$ (Shemmer et al. 2014), deviates from the general trend by an apparently significant amount, despite the relatively large spread around the average relation. Allowing for a gravitational amplification would not change α_{ox}, but changing $L_\nu(2500\,\text{Å})$ could make this object fully consistent with the general distribution, as it occurs in the case of the confirmed lensed QSO 2XMM J091301.0+525929 (see Vagnetti et al. 2010, and references therein). The second clue concerns the Baldwin (1977) effect. With respect to the average negative correlation between the C IV equivalent width (EW) and $\lambda L_\lambda(1350\,\text{Å})$ (Bian et al. 2012), PG 1247+267, with EW = 39.5 Å (Shen et al. 2011), is again deviant and would be brought to full consistency by allowing for gravitational lensing. An amplification of about 10 at the same time would (1) account for both of these effects, (2) bring the Eddington ratio to ∼1, and (3) make this object less luminous than S5 0836+071 and consistent with the τ_l–L relation.

A candidate damped Lyα system (DLA) at $z = 1.223$ in the spectrum of PG 1247+267 was analyzed by Pettini et al. (1999). Although Turnshek & Rao (2002) consider the column density to be too low to classify this absorption system as a DLA, according to the conventional threshold $N_{\rm HI} = 2 \times 10^{20}{\rm cm^{-2}}$, it could be associated with a foreground lensing galaxy. Of course, this does not exclude the fact that anisotropic (close to face-on) emission, possible intrinsic super-Eddington emission, and gravitational lensing occur at the same time. This suggests that we need to further observe the spectral variability to perform velocity resolved RM, and also to investigate lensing evidences. Finally, we note that PG 1247+267 is the fifth most luminous of ∼100,000 QSOs in the Shen et al. (2011) catalog. Among the most luminous objects, the fraction of lensed QSOs may be high enough to bias the SE mass estimates and the studies of the evolution of both the mass function and the Eddington ratio distribution in cosmic time.

We acknowledge funding from PRIN/MIUR-2010 award 2010NHBSBE. M.D. acknowledges PRIN INAF 2011 funding. This research is based on observations collected at the Copernico telescope (Asiago, Italy) of the INAF-Osservatorio Astronomico di Padova, and at the Cassini Telescope (Loiano, Italy) of the INAF-Osservatorio Astronomico di Bologna.

REFERENCES

Alexander, T. 1997, in Astronomical Time Series, ed. D. Maoz, A. Sternberg, & E. M. Leibowitz (Astrophysics and Space Science Library, Vol. 218; Dordrecht: Kluwer), 163
Assef, R. J., Denney, K. D., Kochanek, C. S., et al. 2011, ApJ, 742, 93
Bachev, R., Marziani, P., Sulentic, J. W., et al. 2004, ApJ, 617, 171
Baldwin, J. A. 1977, ApJ, 214, 679
Bentz, M. C., Denney, K. D., Grier, C. J., et al. 2013, ApJ, 767, 149
Bentz, M. C., Peterson, B. M., Netzer, H., Pogge, R. W., & Vestergaard, M. 2009, ApJ, 697, 160
Bentz, M. C., Peterson, B. M., Pogge, R. W., Vestergaard, M., & Onken, C. A. 2006, ApJ, 644, 133
Bessell, M. S. 1990, PASP, 102, 1181
Bian, W.-H., Fang, L.-L., Huang, K.-L., & Wang, J.-M. 2012, MNRAS, 427, 2881
Blandford, R. D., & McKee, C. F. 1982, ApJ, 255, 419
Chelouche, D., Daniel, E., & Kaspi, S. 2012, ApJL, 750, L43
Denney, K. D. 2012, ApJ, 759, 44
Edelson, R. A., & Krolik, J. H. 1988, ApJ, 333, 646
Ferrarese, L., & Merritt, D. 2000, ApJL, 539, L9
Gaskell, C. M. 2009, NewAR, 53, 140
Gaskell, C. M., & Peterson, B. M. 1987, ApJS, 65, 1
Greene, J. E., Peng, C. Y., & Ludwig, R. R. 2010, ApJ, 709, 937
Kaspi, S., Brandt, W. N., Maoz, D., et al. 2007, ApJ, 659, 997
Kaspi, S., Maoz, D., Netzer, H., et al. 2005, ApJ, 629, 61
Kaspi, S., Smith, P. S., Netzer, H., et al. 2000, ApJ, 533, 631
Kelly, B. C., Bechtold, J., & Siemiginowska, A. 2009, ApJ, 698, 895
Kozłowski, S., Kochanek, C. S., Udalski, A., et al. 2010, ApJ, 708, 927
Krawczyk, C. M., Richards, G. T., Mehta, S. S., et al. 2013, ApJS, 206, 4

MacLeod, C. L., Ivezić, Ž., Kochanek, C. S., et al. 2010, ApJ, 721, 1014
Marconi, A., Risaliti, G., Gilli, R., et al. 2004, MNRAS, 351, 169
Marziani, P., & Sulentic, J. W. 2012, NewAR, 56, 49
McGill, K. L., Woo, J.-H., Treu, T., & Malkan, M. A. 2008, ApJ, 673, 703
McIntosh, D. H., Rieke, M. J., Rix, H.-W., Foltz, C. B., & Weymann, R. J. 1999, ApJ, 514, 40
McLure, R. J., & Jarvis, M. J. 2002, MNRAS, 337, 109
Metzroth, K. G., Onken, C. A., & Peterson, B. M. 2006, ApJ, 647, 901
Netzer, H. 2003, ApJL, 583, L5
Netzer, H., Lira, P., Trakhtenbrot, B., Shemmer, O., & Cury, I. 2007, ApJ, 671, 1256
Onken, C. A., Ferrarese, L., Merritt, D., et al. 2004, ApJ, 615, 645
Onken, C. A., & Peterson, B. M. 2002, ApJ, 572, 746
Pancoast, A., Brewer, B. J., Treu, T., et al. 2013, arXiv:1311.6475
Perna, M., Trevese, D., Vagnetti, F., & Saturni, F. G. 2014, AdSpR, 54, 1429
Peterson, B. M. 1993, PASP, 105, 247
Peterson, B. M., Bentz, M. C., Desroches, L.-B., et al. 2005, ApJ, 632, 799
Peterson, B. M., Bentz, M. C., Desroches, L.-B., et al. 2006, ApJ, 641, 638
Peterson, B. M., Ferrarese, L., Gilbert, K. M., et al. 2004, ApJ, 613, 682
Peterson, B. M., & Wandel, A. 1999, ApJL, 521, L95
Peterson, B. M., Wanders, I., Bertram, R., et al. 1998, ApJ, 501, 82
Pettini, M., Ellison, S. L., Steidel, C. C., & Bowen, D. V. 1999, ApJ, 510, 576
Pickles, A., & Depagne, É. 2010, PASP, 122, 1437
Press, W. H., Rybicki, G. B., & Hewitt, J. N. 1992, ApJ, 385, 416
Press, W. H., Teukolsky, S. A., Vetterling, W. T., & Flannry, B. P. 2007, Numerical Recipes, The Art of Scientific Computing, Third Edition (Cambridge: Cambridge Univ. Press), 824
Ramsey, L. W., Adams, M. T., Barnes, T. G., et al. 1998, Proc. SPIE, 3352, 34
Runnoe, J. C., Brotherton, M. S., DiPompeo, M. A., & Shang, Z. 2014, MNRAS, 438, 3263
Runnoe, J. C., Brotherton, M. S., Shang, Z., & DiPompeo, M. A. 2013, MNRAS, 434, 848
Rybicki, G. B., & Kleyna, J. T. 1994, in ASP Conf. Ser. 69, Reverberation Mapping of the Broad-Line Region in Active Galactic Nuclei, ed. P. M. Gondhalekar, K. Horne, & B. M. Peterson (San Francisco, CA: ASP), 85
Rybicki, G. B., & Press, W. H. 1992, ApJ, 398, 169
Saturni, F. G., Trevese, D., Vagnetti, F., & Perna, M. 2014, AdSpR, 54, 1434
Shemmer, O., Brandt, W. N., Paolillo, M., et al. 2014, ApJ, 783, 116
Shen, Y., & Kelly, B. C. 2012, ApJ, 746, 169
Shen, Y., Richards, G. T., Strauss, M. A., et al. 2011, ApJS, 194, 45
Sluse, D., Schmidt, R., Courbin, F., et al. 2011, A&A, 528, 100
Sulentic, J. W., Bachev, R., Marziani, P., Negrete, C. A., & Dultzin, D. 2007, ApJ, 666, 757
Sulentic, J. W., Marziani, P., Zamanov, R., et al. 2002, ApJL, 566, L71
Trevese, D., Paris, D., Stirpe, G. M., Vagnetti, F., & Zitelli, V. 2007, A&A, 470, 491
Trevese, D., Saturni, F. G., Vagnetti, F., et al. 2013, A&A, 557, A91
Turnshek, D. A., & Rao, S. M. 2002, ApJL, 572, L7
Vagnetti, F., Turriziani, S., Trevese, D., & Antonucci, M. 2010, A&A, 519, A17
Vestergaard, M. 2002, ApJ, 571, 733
Vestergaard, M. 2004, ApJ, 601, 676
Vestergaard, M., & Peterson, B. M. 2006, ApJ, 641, 689
Wandel, A., Peterson, B. M., & Malkan, M. A. 1999, ApJ, 526, 579
White, R. J., & Peterson, B. M. 1994, PASP, 106, 879
Zu, Y., Kochanek, C. S., Kozłowski, S., & Peterson, B. M. 2013a, arXiv:1310.6774
Zu, Y., Kochanek, C. S., Kozłowski, S., & Udalski, A. 2013b, ApJ, 765, 106
Zu, Y., Kochanek, C. S., & Peterson, B. M. 2011, ApJ, 735, 80